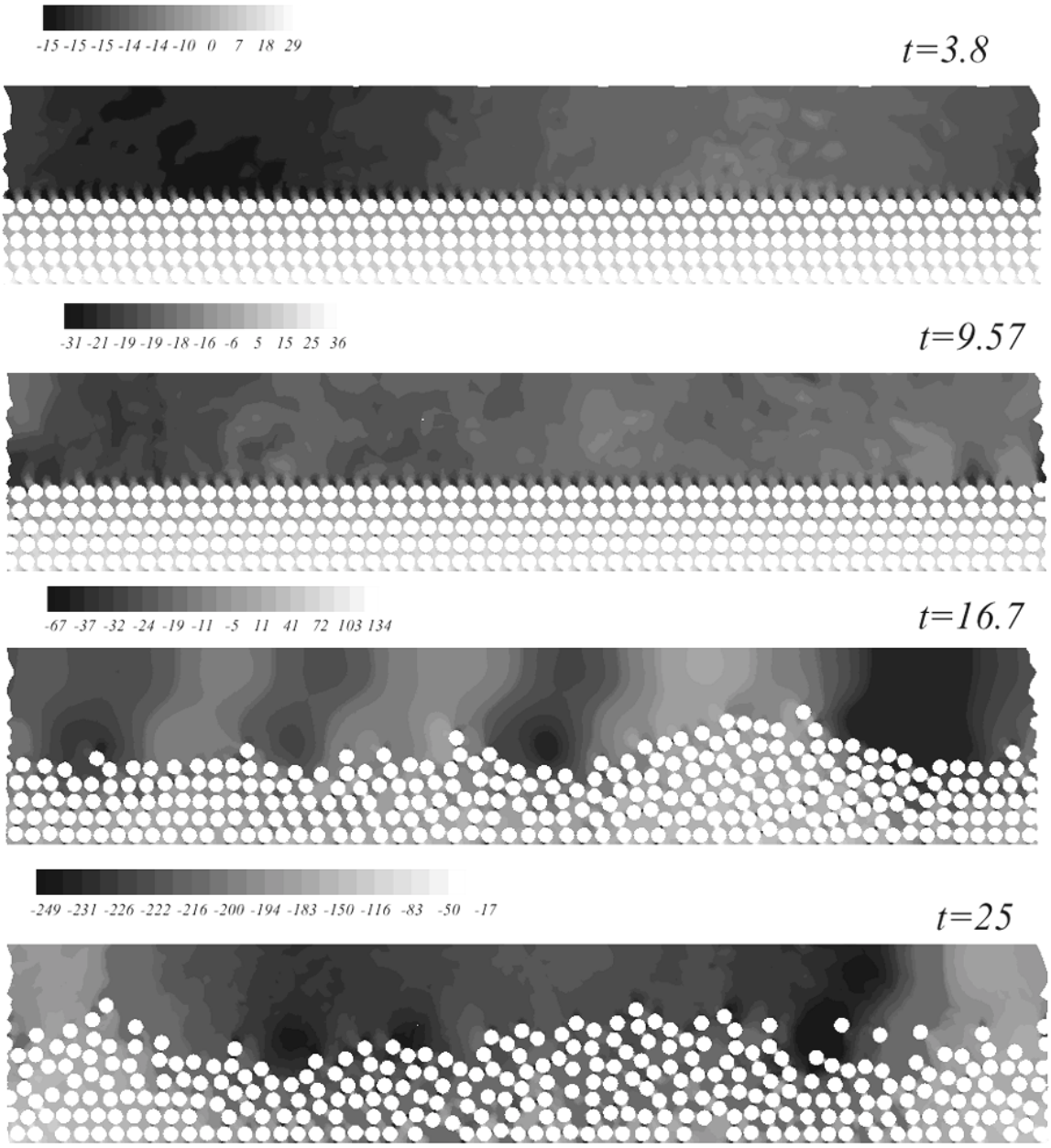

Figure 11. Fluidization of 300 particles (η = 0.2 poise, R *= 150,* G *= 1.63). The final state of the fluidization at* t *= 25 sec has not fully eroded. The particles that lift out of the bed can be described as saltating. A propagating "interfacial" wave is associated with the propagating pressure wave at* t *= 250.*

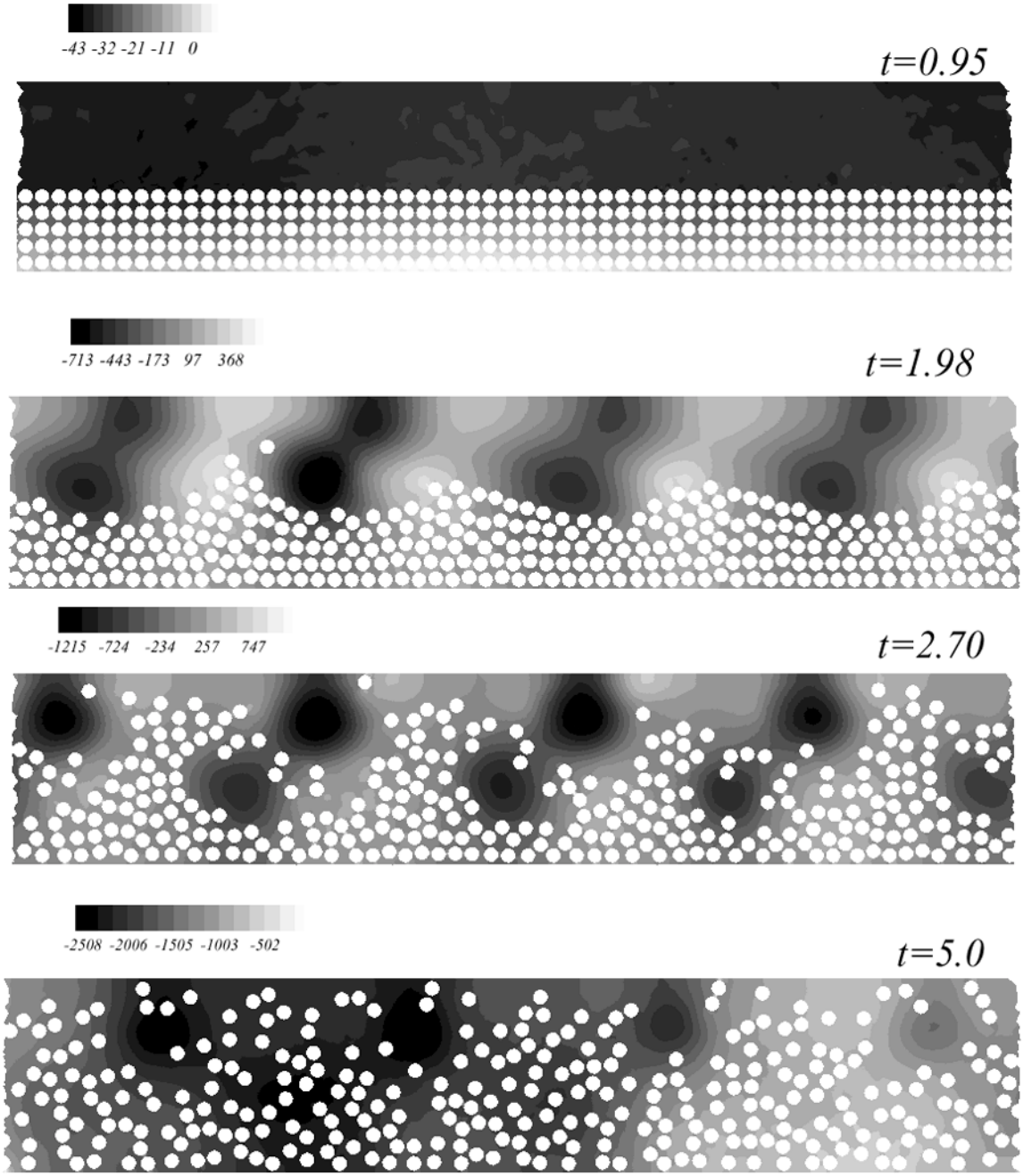

Figure 12. Fluidization of 300 particles (η = 0.2 poise, R *= 450,* G *=0.54). The flow is from left to right. The particles can be lifted to the top of the channel.*

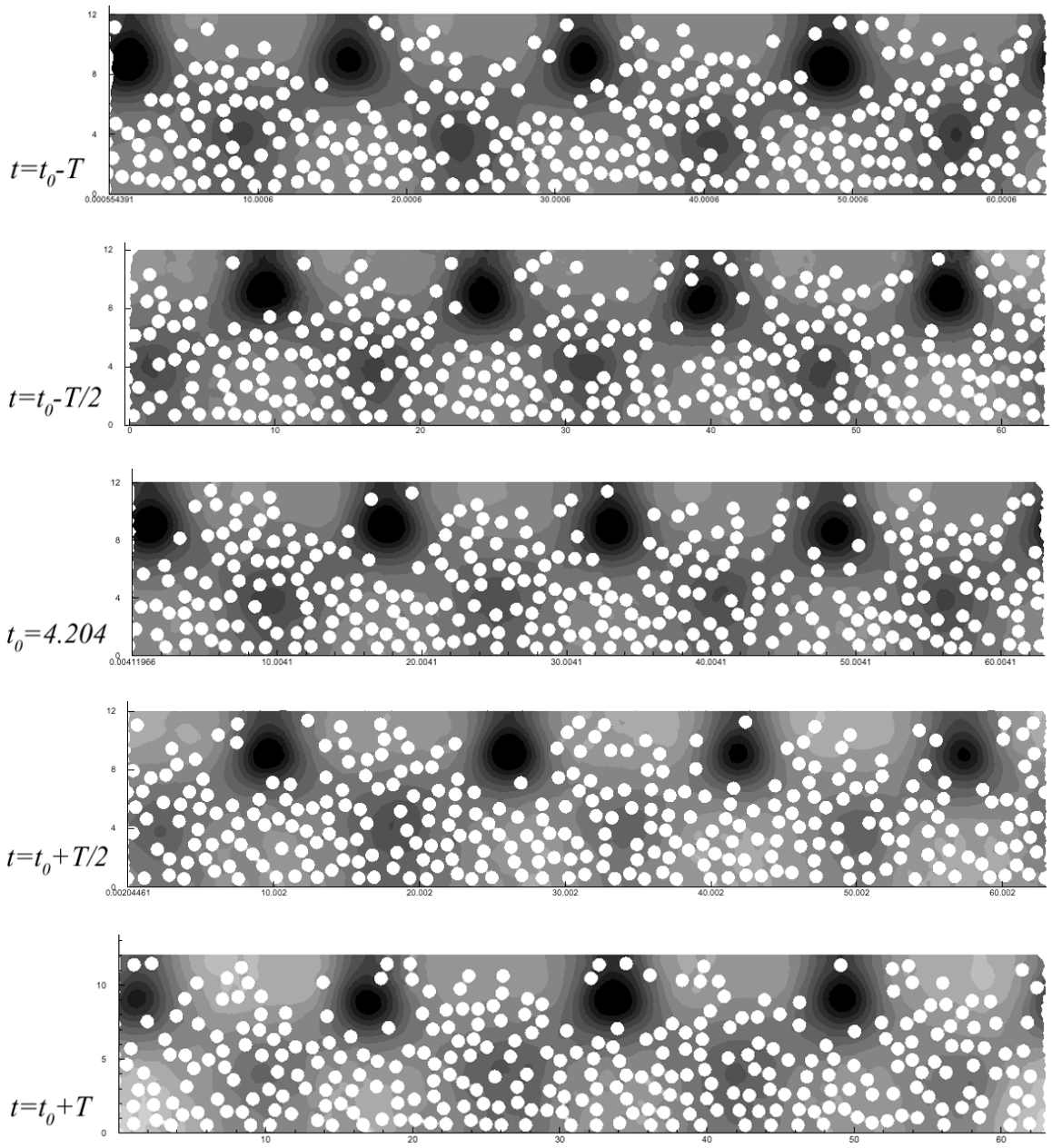

Figure 13. Propagation of the pressure wave centered at t_0 *= 4.204 sec in case* η *= 0.2 poise,* R *= 450 shown in figure 12. The period* T *of this wave is* T *= 0.56 sec and its wavelength is 16 cm.*

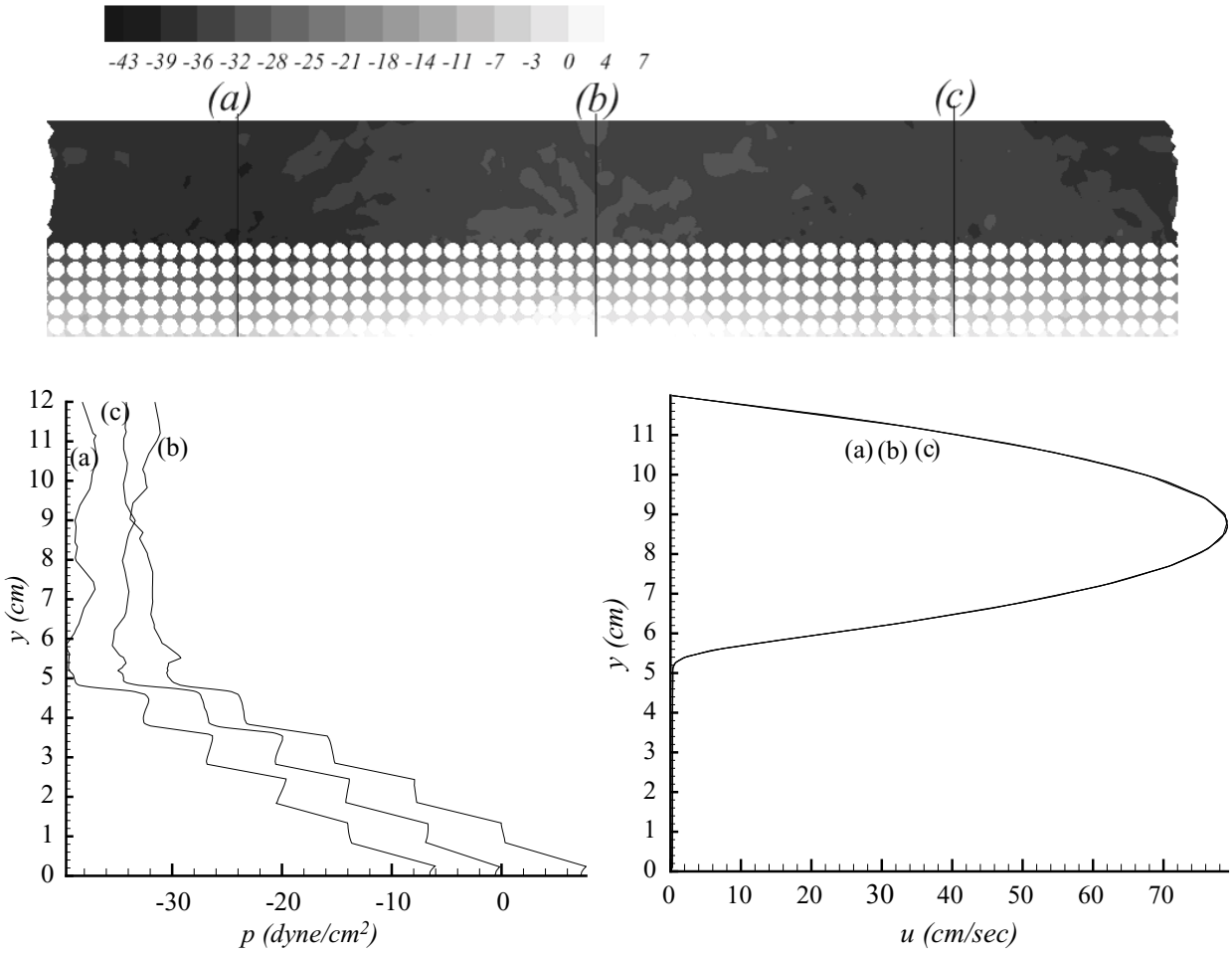

Figure 14. Distribution of dynamic pressure p *and streamwise velocity* u *at* t = *0.1 sec when* R = *350,* η = *0.2 poise. The distribution is basically vertical. This kind of distribution is typical of the earliest times. The vertical steps show how the fluid supports rows of particles. The particles move forward together, with only a small velocity.*

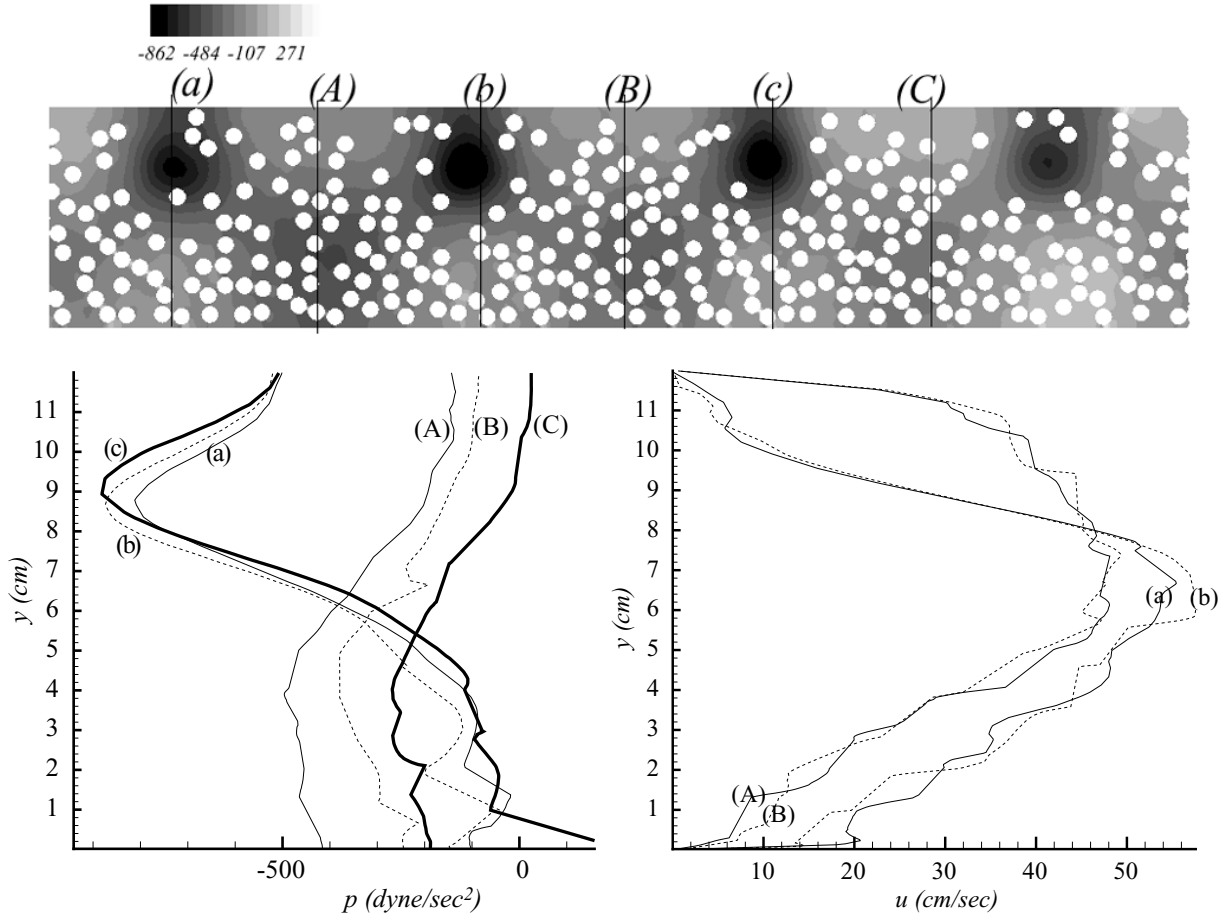

Figure 15. Distribution of dynamic pressure p *and streamwise velocity* u *at* t = *4.95 when* R = *350,* η = *0.2 poise (see figure 12). The pressure and velocity distribution can be associated with "crest" and "trough" propagating void fractions.*

▪ Case 3: η = 0.01 poise, $R_G = 9.81/\eta^2 = 9.8 \times 10^4$

Figure 16 gives the height of center of gravity of 300 particles in water as a function of $R = 6\overline{p}/\eta^2 = 6\times10^4\,\overline{p}$. The interpretation of figure 16 is basically the same as figure 3. Snapshots of the evolution to full fluidization are shown in figures 17 and 18.

The evolution to full fluidization is accomplished by pressure waves. For low Reynolds numbers the bed expansion is small; the snapshot at *t* = 116 sec in figure 17 is an example of bed expansion in water at low *R*. The bed has expanded by the development of voids and dislocations near the top of the bed; only a few particles are fluidized. The bed is not severely eroded.

Fluidization in water at high Reynolds numbers is greatly different. The fully fluidized bed shown at *t* = 0.46 sec in figure 18 is completely eroded. The evolution of the fluidized suspension is driven by a propagating pressure wave, which is in one-to-one correspondence with the propagation of voids. At *t* = 0.27 sec, before the bed has fully fluidized, these voids coincide with wave troughs.

Figure 19 and 20 show how the dynamic pressure p develops as the bed evolves to full fluidization. For this case t = 0.1 sec is not an early time; the periodic pressure pulses which drive particles into suspension have already developed.

Figure 21 focuses on the wave properties of the evolving fluidization of 300 particles in water when R = 1200. The t = 40 sec panel of figure 17 shows a propagating and nearly spatially periodic wave of particles. Wave forms for the dynamic pressure p, the vertical velocity V and the horizontal velocity U are shown.

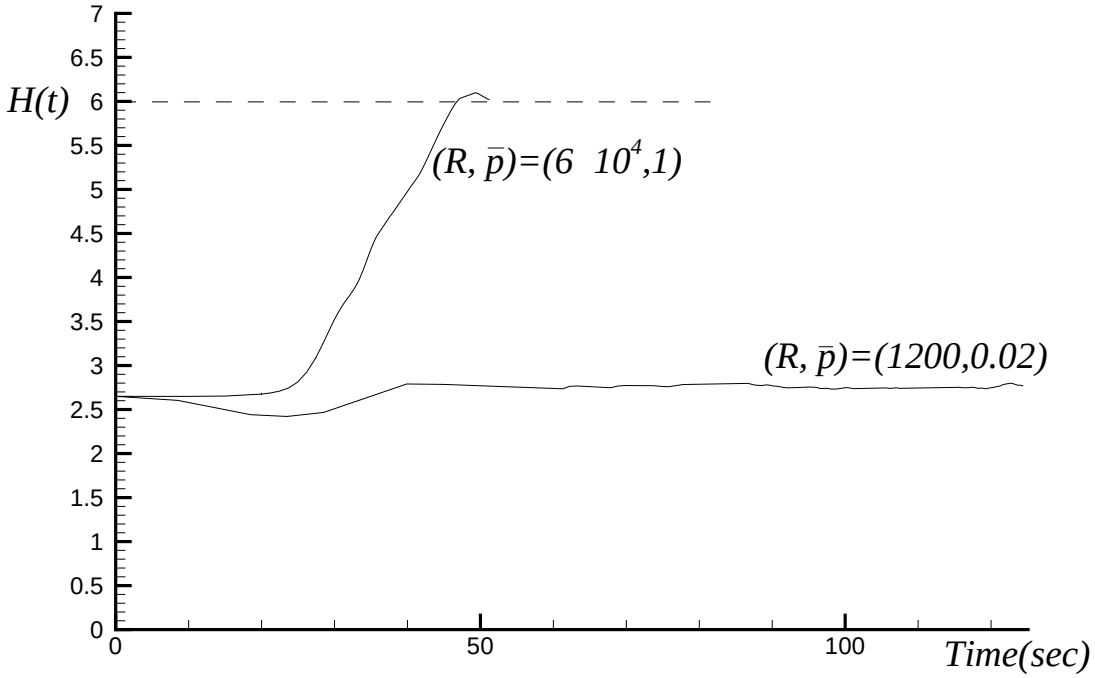

Figure 16. Rise curves for the center of gravity of 300 circular particles fluidized by lift (η = 0.01, RG = 9.81/ η^2 = 9.81 $\times$ 10^4). $\bar{p}$ is in dyne/cm^2. The time scale for the fast rise at $\bar{p}$ =1.0 has been expanded by 100; the real time corresponding, say, to 50 is 0.5sec. The rise to full fluidization is very rapid and at full fluidization the mass center of the particles is closer to the top than to the bottom wall. The bed inflation at R = 1200 is modest; at early times the position of the mass center actually decreases because the circles are more efficiently packed. (hexagonally, rather than cubically packed at t = 27.)

Table 3. Data for the forward motion of a fluidized suspension of 300 particles after the bed has fully inflated and the average height $\bar{H}$ of all particles has stopped increasing (η = 0.01). $\bar{H}$ = $\bar{H}_0$ = 2.65d at t = 0. $\bar{U}$ and $\bar{\Omega}$ are the average velocity and angular velocity of particles.

R	R_g	$\bar{p}$	$\bar{H}$	$\bar{U}$	$\bar{\Omega}$
1200	81.75	0.02	2.77	0.63	0.04
6×10^4	1.64	1.0	6.02	116.20	4.50

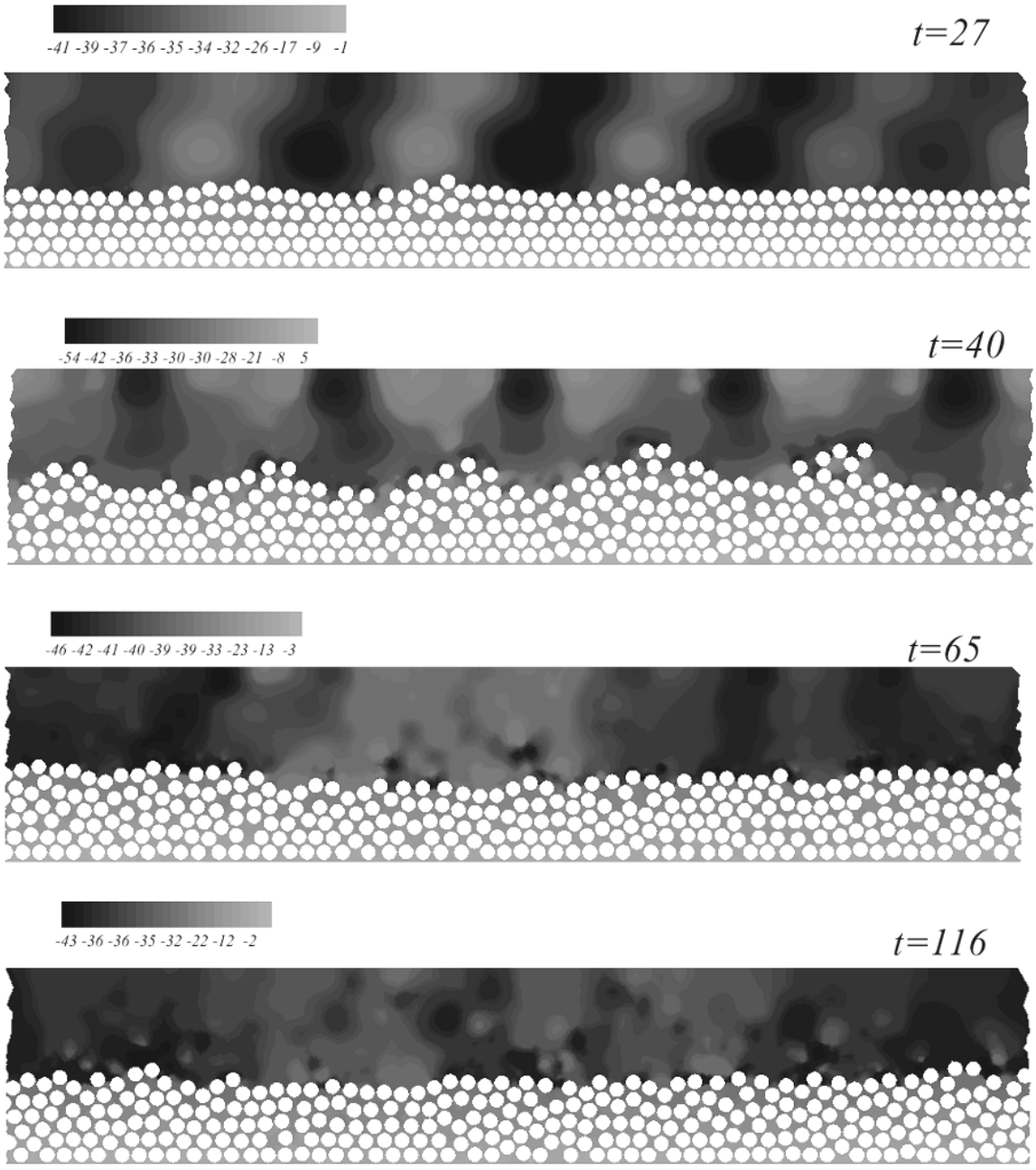

Figure 17. Fluidization of 300 particles (η = 0.01 poise, R = 1200, G = 81.75). The flow is from left to right. This is a "relatively" heavy suspension with a smaller value of R/G. At t = 27 the flow packs the

initial cubic array more closely into a hexagonal array and the mean bed height drops. The final fluid condition for t > 116 is mildly inflated, more closely packed at the bottom than the top.

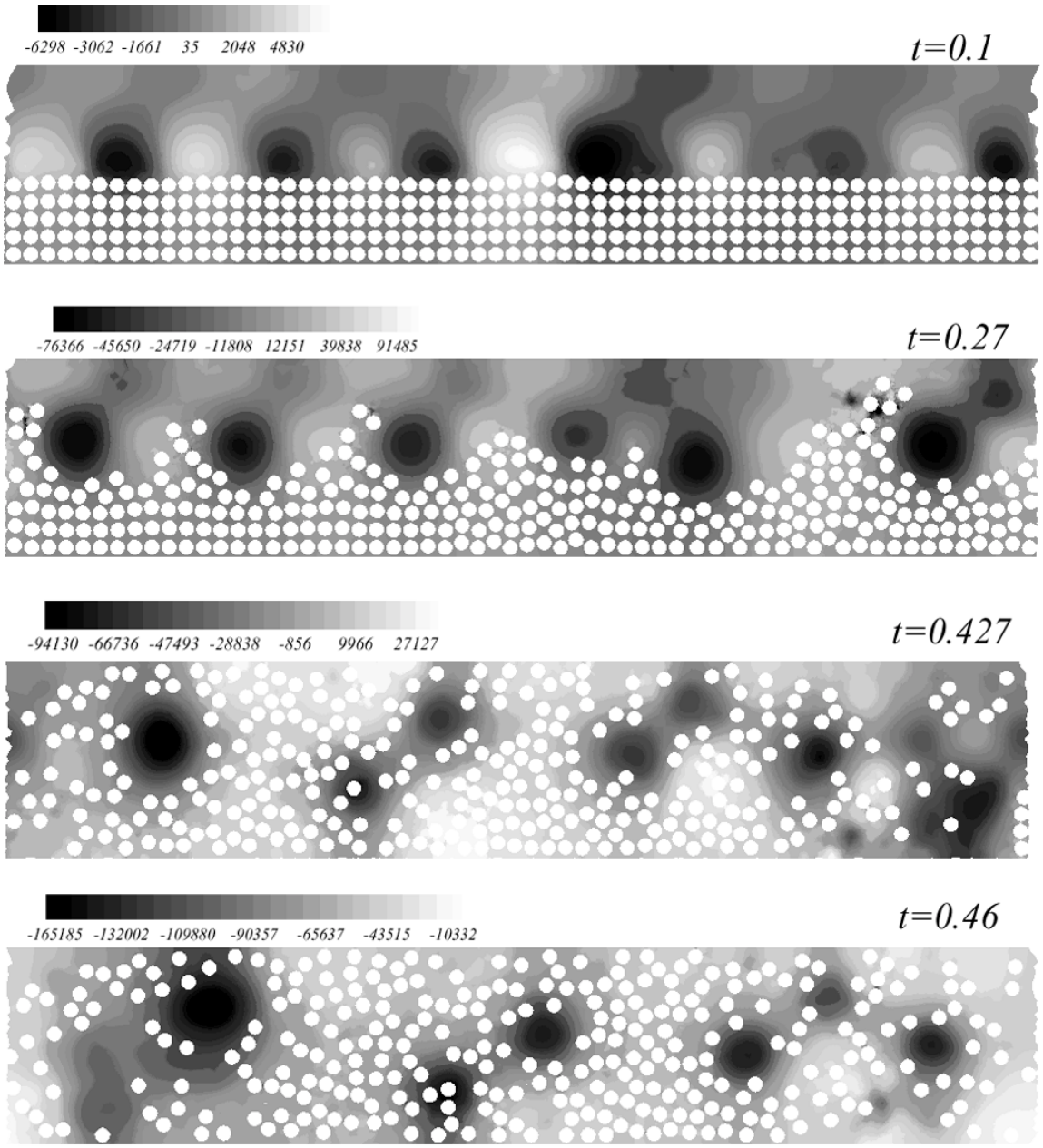

Figure 18. Fluidization of 300 particles in water (η = 0.01 poise, R = 6 $\times$ 10^4, G = 1.64), This is a "relatively" light suspension with a much larger value of R/G. Particles fluidize easily; the mean bed height is higher than mid-channel.

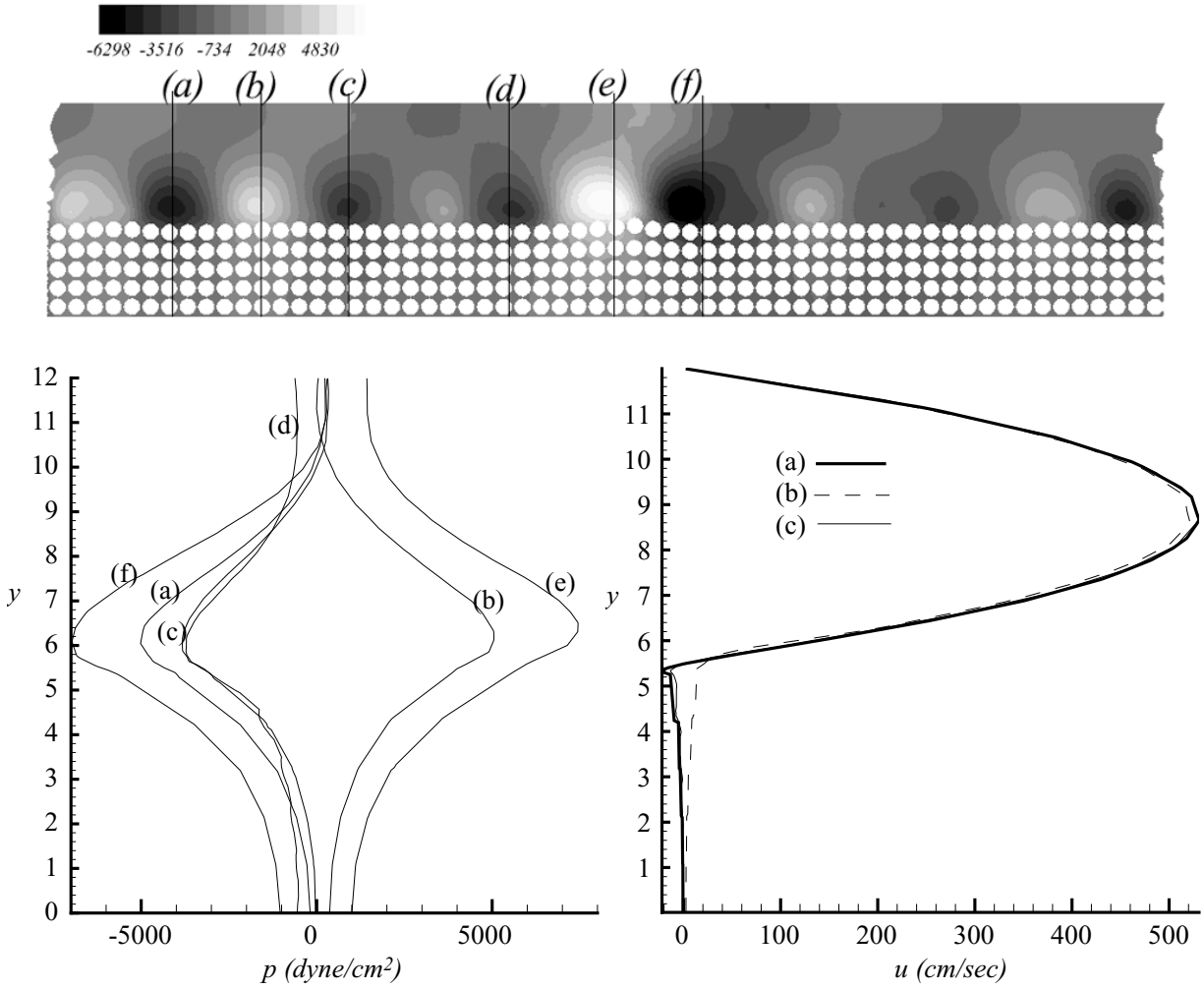

Figure 19. Distribution of dynamic pressure p *and streamwise velocity* u *at* t = *0.1 sec for the fluidization of 300 particles in water when* R = 6×10^4 *(see figure 18). In this case* t = *0.1 sec is not an early time; the propagating pressure wave has already developed, but it does not yet have a big effect on the velocity distribution.*

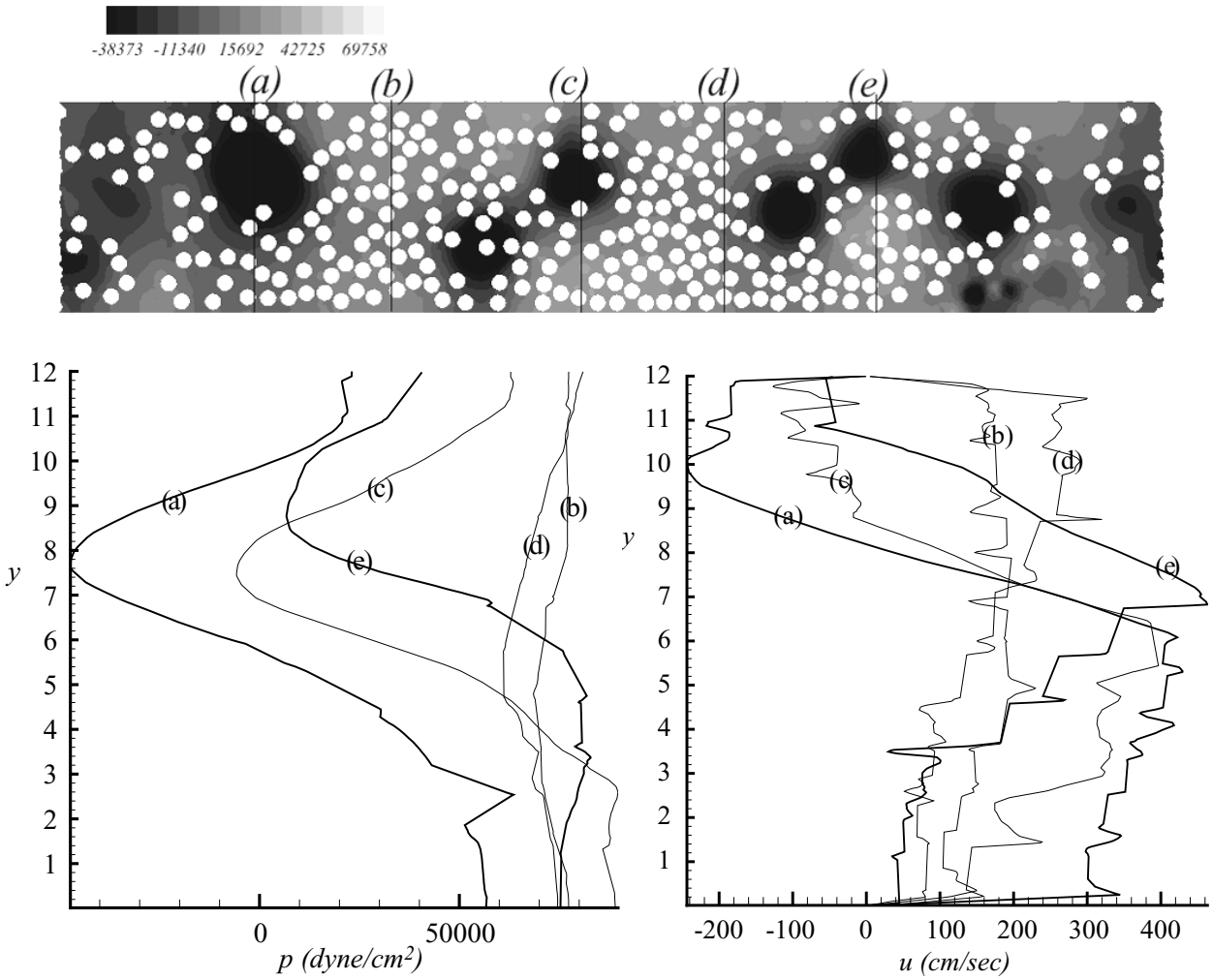

Figure 20. Distribution of dynamic pressure p *and streamwise velocity* u *at* t = *0.46 sec (see figure 18). The pressure and velocity wave coincides with the propagation of internal waves of void fractions.*

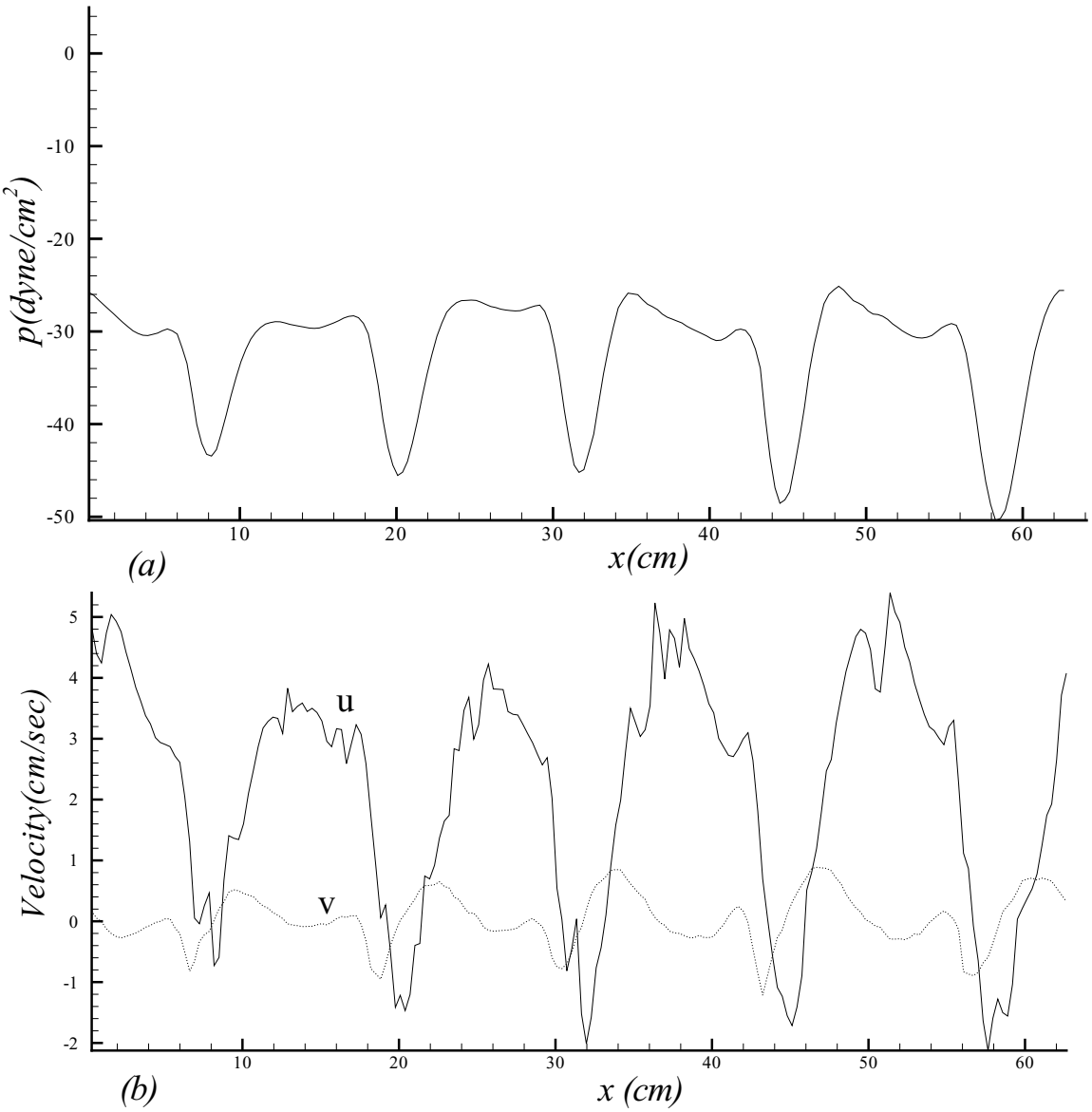

Figure 21. (a) Distribution of dynamic pressure p*, (b) vertical velocity* v *and horizontal velocity* u *in water near the upper wall (*y *= 11 cm) at* t *= 40 when* R *= 1200,* G *= 81.75, see figure 17). These spatially periodic waves propagate.*

▪ Inertial mechanism of fluidization

We studied the fluidization of 300 circular particles in a Poiseuille flow. Initially the particles are arranged in a cubic array filling nearly half the channel. The flow breaks the cubic array and inflates the bed by pumping liquid into the bed. The pressures that develop in the bed can levitate the particles. Bed inflation may be divided into two regimes; an eroded bed in which only the top rows of the bed have been inflated, and a fully fluidized bed in which all of the particles are supported by lift forces from the fluid flow. The pumping of liquid into the bed at the earliest times appears to be a universal inertial effect associated with potential flow around spheres and circles. This inertial effect produces high pressure at the front and low pressure at the back side of each circle in the top row of the array. This produces a pressure differential front to back

creating a flow into and out the bed, which dislodges particles from the top row. Further fluidization is driven by the development of a periodic wave of pressure and number density which are clearly evident in the snapshots of the bed evolution.

Apart from aspect and density ratios, the dimensionless equations are fully specified by the values of a shear Reynolds number $R = \dot{\gamma} w d^2 / \nu$ and a gravity number $G = d(\rho_p - \rho_f)g / \dot{\gamma}_w \eta$ and the number of particles in the cell. The ratio *R/G* is independent of η and can be viewed as the ratio of lift to buoyant weight whereas the product *RG* is independent of $\dot{\gamma}_w$ and can be regarded as the ratio of buoyant to viscous damping; you get rapid bouncing around when *RG* is large and high lifts, high average height and very inflated beds when *R/G* is large. A summary of the average height, velocity and angular velocity of the particles in the fully inflated beds for η = 1, 0.2 and 0.01 poise are presented in tables 1~3.

▪ Model of slip velocity

In the modeling of solid-liquid flows the slip velocity is an important but sometimes ambiguous quantity. For single particle lift studies the slip velocity is defined as the difference between the fluid velocity at the particle center when there are no particles and the particle velocity. When there are many particles other possibilities become viable. For example, in the well known drift flux model (see Wallis 1969) drift velocities are defined as the difference between the component velocities and the composite velocity. This kind of definition is useful when there is large difference in the average solid and liquid velocity. In sedimenting suspensions and in suspensions fluidized by drag these large differences arise from the back flow which is absent in suspensions fluidized by lift. For such suspensions the concept of "slip" needs analysis.

Joseph [2000] proposed a model problem for plane Poiseuille flow defined in figure 22 in which we replace the circle of diameter d with a long rectangle whose short side is d. the rectangle is so long that we may neglect effects of the ends of the cylinder at sections near the cylinder center. The midplane of the cylinder is a distance y_1 from the bottom wall and

$$y_1 > d/2, \quad W - y_1 > d/2 \tag{4.1}$$

When no particle is in the flow

$$u = \frac{\overline{p}}{2\eta} y(W - y) \tag{4.2}$$

The long particle is moved forward by shear from the Poiseuille flow at a speed U_p which we shall obtain from the particles equation of motion (4.9) for steady flow. When $0 \le y \le y_1 - d/2$ we find

$$u = \frac{\overline{p}}{2\eta} y\left[y_1 - \frac{d}{2} - y \right] + \frac{U_p y}{y_1 - d/2} \tag{4.3}$$

And when $y_1 + d/2 \le y \le W$ we have

$$u = \frac{\overline{p}}{2\eta}(y - W)\left[y_1 + \frac{d}{2} - y \right] + \frac{U_p (y - W)}{y_1 + d/2 - W} \tag{4.4}$$

For the force balance consider the long rectangle whose long side is L and its short side is d, as in figure 22. The cylinder moves forward with steady velocity U_p. The cylinder is impelled forward by the pressure force $(p_1 - p_2)d$ and is resisted by a shear force from the fluid motion

$$\left(\tau_{xy}\Big|_{y_1 + d/2} - \tau_{xy}\Big|_{y_1 - d/2} \right) L = \eta \left(\frac{du}{dy}\Big|_{y_1 + d/2} - \frac{du}{dy}\Big|_{y_1 - d/2} \right) L \tag{4.5}$$

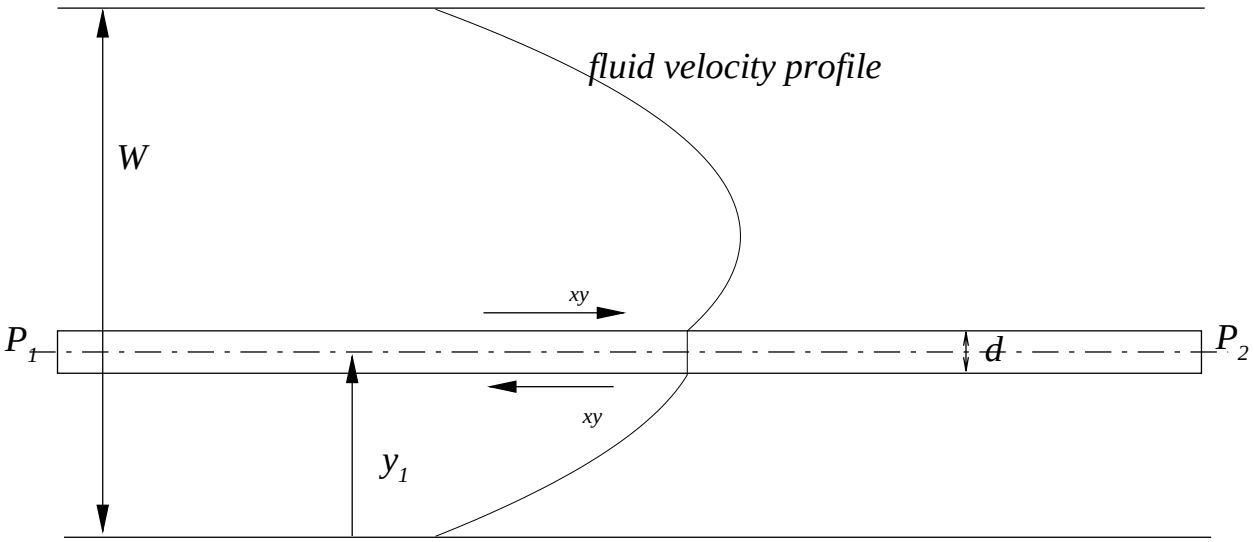

Figure 22. Forces on long particle in a steady Poiseuille flow.

Equating the pressure and shear forces, after dividing by L and writing $(p_1 - p_2) / L = \bar{p}$, we get

$$\bar{p}d = \eta \frac{du}{dy}\Big|_{y_1 - d/2} - \eta \frac{du}{dy}\Big|_{y_1 + d/2} \tag{4.6}$$

where

$$\frac{du}{dy}\Big|_{y_1+d/2} = -\frac{\bar{p}}{2\eta}\left(y_1 + \frac{d}{2} - W \right) + \frac{U_p}{y_1 + d/2 - W} \tag{4.7}$$

and

$$\frac{du}{dy}\Big|_{y_1-d/2} = -\frac{\bar{p}}{2\eta}\left(y_1 - \frac{d}{2} \right) + \frac{U_p}{y_1 - d/2} \tag{4.8}$$

After combining the last three equations we find that

$$U_p = \frac{\bar{p}}{2\eta}\left\{ \frac{W+d}{W-d}\left(y_1 - \frac{d}{2} \right)\left(W - y_1 - \frac{d}{2} \right) \right\} \tag{4.9}$$

When d → 0

$$U_p \rightarrow \frac{\bar{p}}{2\eta} y_1 (W - y_1) \tag{4.10}$$

which is the value $U(y_1)$ of the fluid velocity given by (4.2).

We next evaluate the slip $U(y_1) - U_p$ forming the ratio

$$\frac{U_p}{U(y_1)} = \left(\frac{W+d}{W-d}\right)\left(\frac{y_1 - d/2}{y_1}\right)\left(\frac{W - y_1 - \frac{d}{2}}{W - y_1}\right) \tag{4.11}$$

To show that $\frac{U_p}{U(y_1)}$ is less than 1 when $d>0$, we note that

$$(W-d)y_1(W-y_1) - (W+d)(y_1 - d/2)(W - y_1 - d/2)$$
$$= (y_1 - W/2)^2 + \frac{d}{8}(W-d) > 0$$

In our simplified model the fluid velocity is larger than the particle velocity in steady flow and the lag increases as the particle diameter increases. Small particles follow the fluid with vanishing lag.

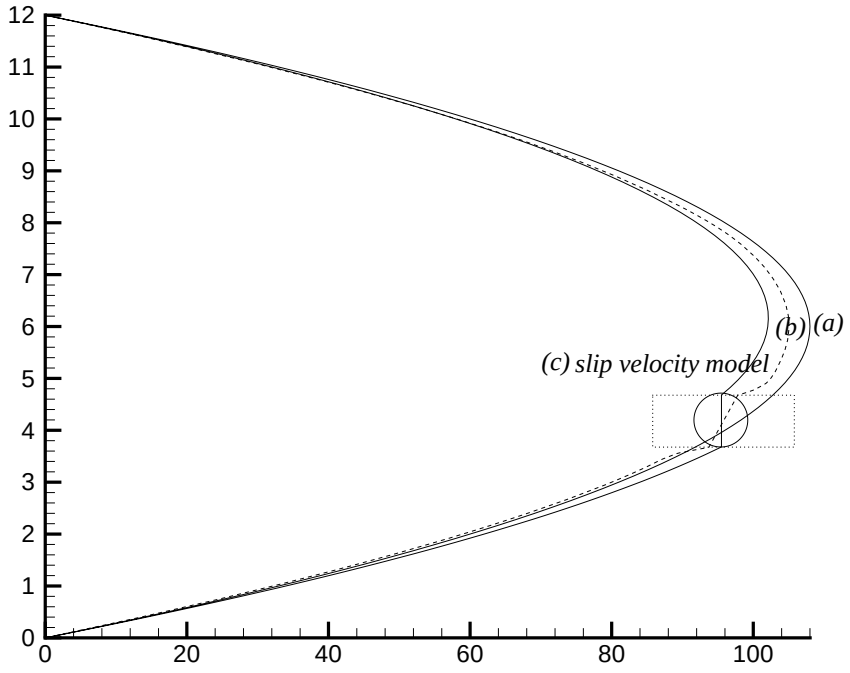

Figure 23. Velocity profiles for three different solutions with W = 12 cm, d = 1 cm, η = 0.2 poise and $\overline{p}$ = 1.2 dynes/cm^3. (a) Undisturbed Poiseuille flow (b) DNS one circular particle h_e = 4.18 cm (see Table 1) (c) model problem corresponding to figure 22 with y = 4.18 cm. The model reduces the velocity much more because the particle is long and because it does not rotate.

The calculation just given suggests that the presence of even one particle can produce a global change of the fluid velocity. This kind of global change can be generated by circles as is shown in figures 23 and 24. The velocity profiles far upstream and downstream of the particle tend to undisturbed values. The effect of particle rotation is to diminish the effect of the particle on the fluid motion. Our long particle cannot rotate but we could express an effect of rotation by

allowing for a shear profile, less than the shear in the unperturbed fluid, in the long body as if it were a very viscous fluid. The shear in the very viscous fluid would be greater than the zero shear of the solid and less than the shear in the undisturbed flow. The difference between the shear in the undisturbed fluid and the very viscous fluid can be viewed as representing the angular slip velocity. The "no shear" solid corresponds to a circular particle for which rotation is suppressed.

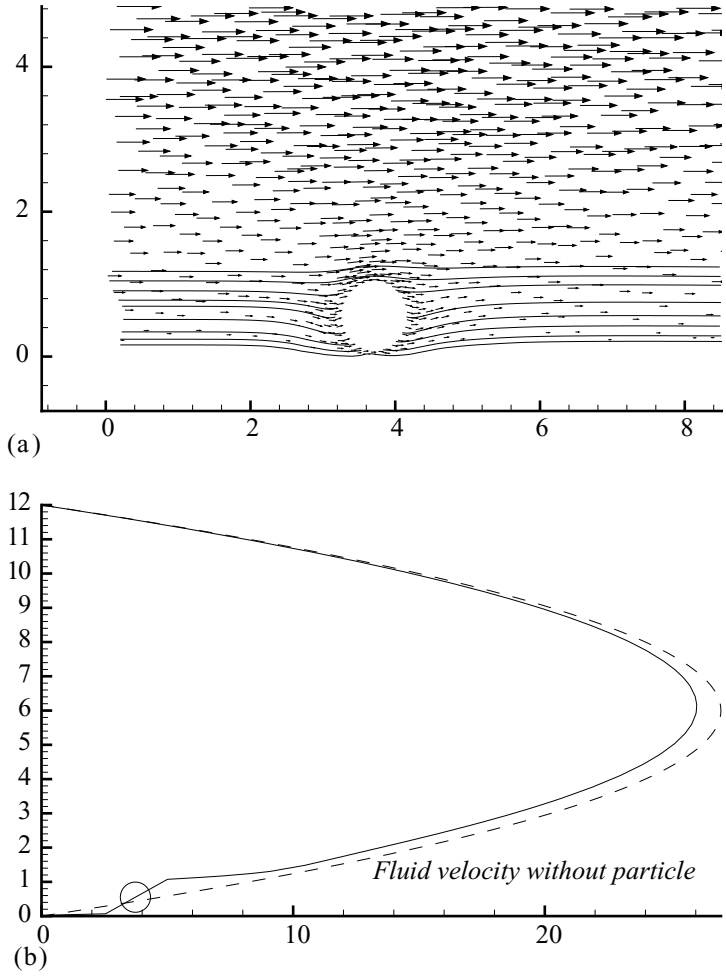

Figure 24. Velocity for the steady flow of a levitated particle near the wall (R = 45, G = 5.4, η = 0.2, $\overline{p}$ = 0.3; see table 2.) (a) velocity vector and streamlines (b) velocity profile on the vertical line through the particle center.

The presence of more than one particle produces yet more lag globally and the best way to see the change is to compare the profile with the undisturbed flow. In figure 25 we have used tecplot to plot profiles at 6 different sections of the flow of 300 particles at $\overline{p} = 20\,\text{dyne/cm}^3$, t = 28 sec identified by vertical lines in figure 7. The open circles give the velocity at fluid points. The straight line segments pass through particles which are rotating. There is no slip velocity in such a plot; the velocity is continuous through the particle.

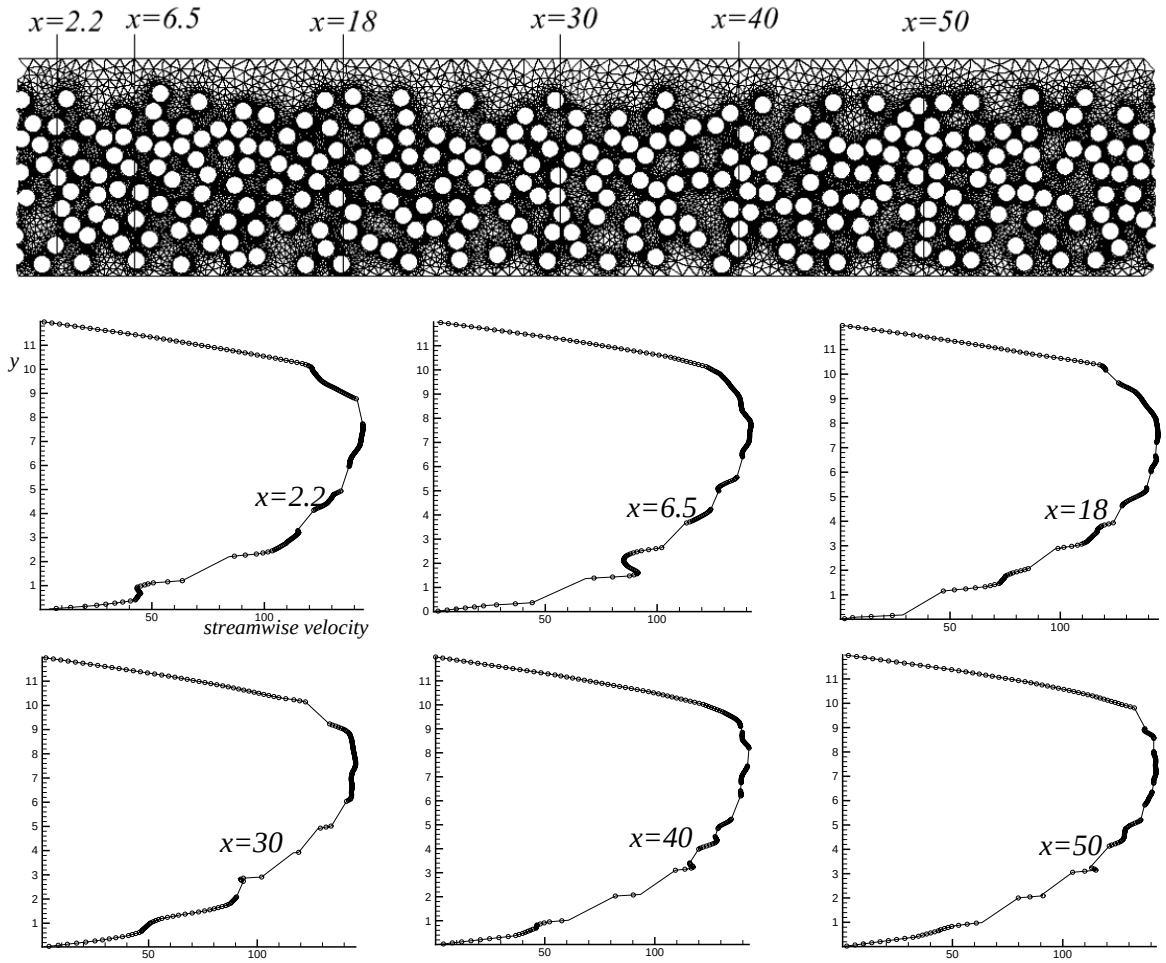

Figure 25. Fluid velocity profiles at 6 different sections of the flow of 300 particles at $\overline{p}$ *= 20 dyne/cm*^{3}*,* η *= 1.0 and when it is fully fluidized (t = 28).*

In figure 26 we plotted the 10 average fluid velocities as a function of *y*. They are obtained by averaging fluid velocities at about 1000 points of *x* coordinate at a fixed *y*. These averages are shown as 10 black circles. A scatter plot of particle velocities is shown and a polynomial fit to this scatter plot is given as a light solid. There does not seem to be a large difference between the average fluid velocity and the average solid velocity defined in this way, but a small positive difference between the fluid and particle velocities is vaguely evident. On the other hand, the difference between the composite fluid-solid velocity and the particle free Poiseuille flow profile is dramatic.

The data shown in figure 26 suggests that one of the main effects of particles in a fluid is to radically reduce the velocity of the composite. Each particle produces a drag on the fluid in a freely moving suspension. The effect of such a distributed drag is equivalent to some form of effective viscosity. Algorithms for the construction of such effective viscosities would find many important applications. Unfortunately the empirical forms of effective viscosity functions which work well for uniform fluidized and sedimenting suspensions work much less well for sheared suspensions.

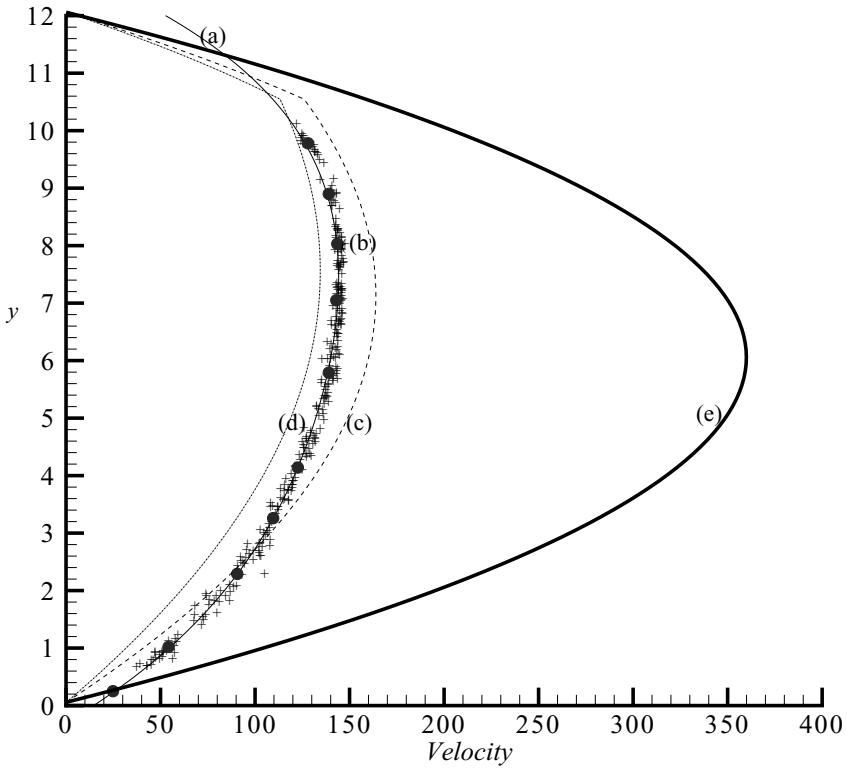

Figure 26. Scatter plot of particle velocities (+) of 300 particles taken from figure 25 (η = 1 poise, $\bar{p}$ = 20 dyne/cm^3); (a) average particle velocity for the scatter (—); (b) average fluid velocity taken from the tecplots in figure 25 at 10 values of y over 1000 points; (c) two-fluid Poiseuille flow model based on (4.14) and (4.15) using the effective viscosity η_m = 3.06 from (4.12) with ϕ = 0.36 and (d) η_m = 4.19 from (4.13); (e) undisturbed Poiseuille flow. The particles "hold up" the fluid. The increased drag on the fluid due to the free particles can be modeled as an effect of an increased viscosity of the fluid-solid mixture.

For comparison, we calculated velocity profiles using a two-fluid effective viscosity theory. We suppose that the particle-laden region is an effective fluid with an effective viscosity and an effective density, though the effective density is not needed for the calculation to follow. The selection of the region occupied by the fluid-solid mixture is somewhat arbitrary. We suppose that the mixture has a uniform volume fraction under a flat interface of height $2\bar{H}$ where $\bar{H}$ is the mean height. The volume fraction is obtained as $300\pi d^2/8\bar{H}L$ where *d=1cm, L=63cm.* Two highly regarded expressions for the effective viscosity of a uniform suspension of spheres of volume fraction ϕ are:

$$\eta_m = \eta_f/(1-\phi/A)^2,\ A=0.638 \tag{4.12}$$

which is due to Kataoka et al.[1978] into two dimension and

$$\eta_m = \eta_f(1+2.5\phi+10.05\phi^2+0.00273e^{16.6\phi}) \tag{4.13}$$

which is due to Thomas [1965]. These expressions were obtained from experiments and may not apply in two dimensions. We used $A = A_{2D} = 0.8328$ which scales A into two dimension in the ratio of close packed hexagonal packings in 2 and 3 dimensions $A_{2D} = \frac{0.907}{0.740} A_{3D}$. The effective theory is a two-fluid stratified Poiseuille flow satisfying the following equations

$$\bar{p} = \eta_f \frac{\partial^2 u_f}{\partial y^2} \quad \text{for } y \geq h, \qquad \bar{p} = \eta \frac{\partial^2 u_m}{\partial y^2} \quad \text{for } y \leq h \tag{4.14}$$

where $h = 2\overline{H}$ is the interface between the pure fluid and the mixture. At the boundary

$$\begin{aligned} &u_f(W) = 0.0,\ u_m(0) = 0.0 \text{ and the velocity and shear stress are continuous on } y = h; \\ &u_f(h) = u_m(h) \\ &\eta_f \frac{\partial u_f}{\partial y}(h) = \eta \frac{\partial u_m}{\partial y}(h). \end{aligned} \tag{4.15}$$

The comparison of the effective theory corresponding to (4.12) and (4.13) with the numerical simulation is exhibited in figure 26. The agreement between the effective theory and the simulation is far from perfect but there is agreement within a large tolerance. The effective theory however has several big defects which must be overcome before it can be used to model the slurry; first and foremost the theory requires that *h* be specified; here from the simulation a second problem is that the effective viscosity for uniform suspension need not be a good representation of sheared suspension. It is certain the effective density of the slurry must enter into the height of the fluidized slurry in ways we don't yet understand.

The small difference between the spatially averaged fluid and solid velocities cannot be said to be clearly evident at all positions on a cross section. It is our position that a positive slip velocity is required to support the buoyant weight of particles. In fact, we would expect that the difference between the particle weight and the composite density $\overline{\rho}(\phi) = \rho_p\phi + \rho_f (1- \phi)$ is a factor in the unknown formula for the lift on a particle in a swarm of volume fraction ϕ. In the present case $\rho_p - \overline{\rho}(\phi) = (\rho_p - \rho_f)(1- \phi) = 0.01(1- \phi)$ is very small and a large slip velocity is not required to levitate a particle. The calculation of the slip velocity ought to be defined in terms of time or ensemble averages at a fixed point, which are not readily calculated with the ALE method used here.

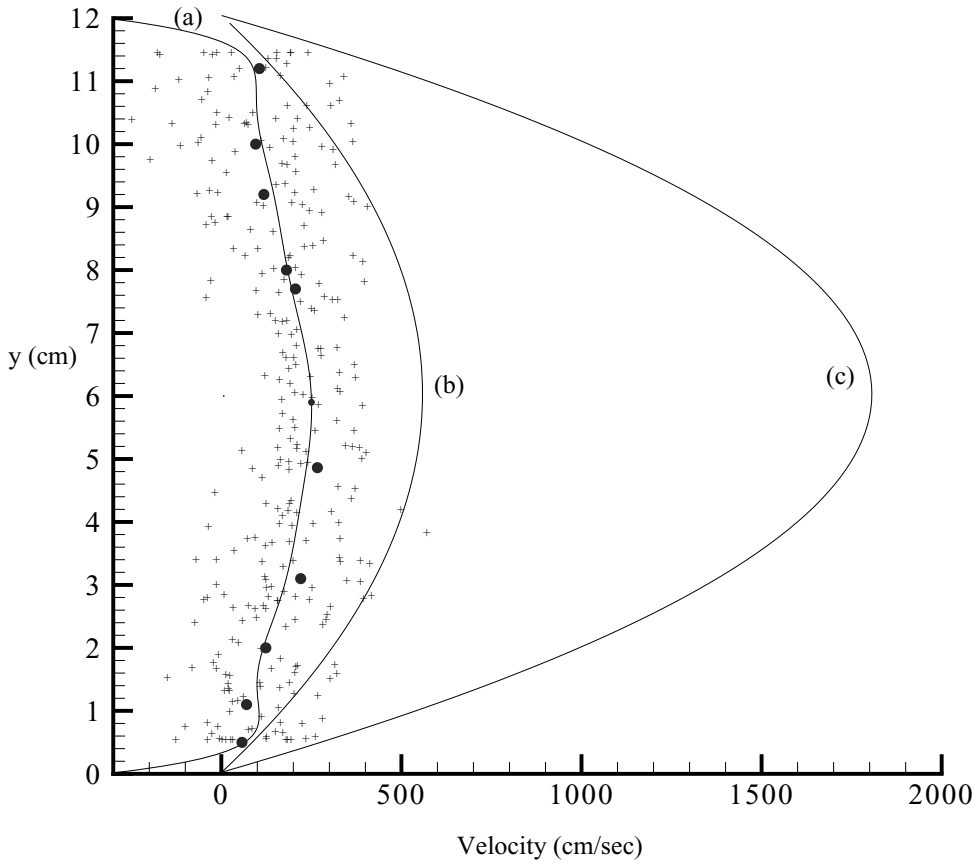

Figure 27. Scatter plot for the fluidization of 300 particles in water (h = 0.01 poise) shown in figure 18. In this case, particles fill the whole channel and the scatter is caused by large fluctuations. (a) The average velocity profile (—) is rather flat as would be expected from turbulent flow. The black dots • are average fluid velocities from the tecplots in figure 18. (b) Velocity profile for Poiseuille flow of a fluid with effective viscosity η_m = 0.032 given by (4.13) for ϕ = 0.31. This does not agree with the simulation. Perhaps it would be better to create an effective "eddy viscosity" theory for this weakly turbulent flow. (c) Undisturbed Poiseuille flow without particles.

Figure 27 gives a scatter plot for the water flow in figure 18 (η = 0.01 poise, $R = 6\times10^4$, G = 164). The results here are what might be expected of turbulent flow and appear to represent the natural extrapolation of results given in this paper at lower Reynolds numbers. The relevant Reynolds number, based on the average particle velocity $\overline{U} = 200\,\text{cm/sec}$, the effective viscosity η_m = 0.032 poise and particle diameter d, is about 6000, a value at which one might expect weak turbulence. Informed readers will question the validity of our computation using Choi's [2000] split method in direct numerical simulation with no artificial viscosity or turbulence model. The natural way to test this result is to do mesh refinement. Our unstructured mesh is generated automatically from nodes on the surface of the circular particle. Our calculation converged, and converged solutions have nearly the same height history for 15 to 30 nodes on the circular particle when the time step size (Δt) used is about 10^{-5} (the corresponding Courant number is about 0.1); the converged solution cannot be obtained when the number of nodes is less than 12 or sometimes greater than 30. When the number of nodes is greater than 30, the calculation may stop because the mesh generator is unable to generate mesh due to the distortion of very short elements during motion. Certainly we have not established the validity of such a high Reynolds

number computation, but the results do converge to something which appears reasonable and survives tests of mesh refinement.

5 Summary of results

1. A numerical package (H. Choi [2000]) based on a splitting method, which is an extension of the numerical package developed by Hu, Joseph and Crochet [1992] for the direct numerical simulation of solid-fluid mixtures, is used to study the fluidization by lift of 300 particles.
2. The present problem is governed by a shear Reynolds number R and a gravity number G. The product $R_G = RG$ is a Reynolds number based on the sedimentation velocity of a sphere under gravity. This is a measure of the activity level and is small when the viscosity is large. The ratio R/G is a generalized Froude number; it compares the inertial lift due to the shear to the buoyant weight and is independent of viscosity; the rise of particles is large when this number is large even though the motion may be sluggish.
3. A turning point bifurcation of a steady forward flow of a single particle was found; the height and particle velocity change strongly at such points and the solutions may exhibit hysteresis. The proof that the arrangement of stable and unstable solutions is associated with double turning points is given in the paper by N. Patankar et el. [2000]
4. The transport of a slurry of 300 particles heavier than liquid particles in a plane pressure driven flow was studied using DNS. Time histories of fluidization if the particles for three viscous fluids with viscosity η = 1.0, 0.2 and 0.01 (water) were computed at different pressure gradients. The time history of the rise of the mean height of particles at a given pressure gradient is monitored and the rise eventually levels off when the bed is fully inflated. The time taken for full inflation decreases as the pressure gradient (or shear Reynolds number) increases. The bed does not inflate when the critical value is below the critical value for lift off of a single particle.
5. At early times, particles are wedged out of the top layer by high pressure at the front and low pressure at the back of each particle in the top row .
6. The dynamic pressure at early times basically balances the weight of the particles in the rows defining the initial cubic array. This vertical stratification evolves into a horizontally stratified propagating wave of pressure which tracks waves of volume fraction. The pressure wave is strongly involved in the lifting of particles. For low viscosity fluids like water where RG is large the particle-laden region supports an “interfacial” wave corresponding to the wave of pressure. If R/G is large the interface collapses since the stronger lift forces push wave crests into the top of the channel, but the pressure wave persists.
7. A simple analytic model for the free motion of a single particle of diameter d in Poiseuille give rise to a formula for the particle velocity

$$\frac{U_p}{U(y_1)} = \left(\frac{W+d}{W-d}\right)\left(\frac{y_1 - d/2}{y_1}\right)\left(\frac{W - y_1 - \frac{d}{2}}{W - y_1}\right.$$

where y_1 is the distance from the channel bottom to the particle center, $U(y_1)$ is fluid velocity at y_1 when no particle is present and *W* is the channel height. The slip velocity $U(y_1) - U_p > 0$ is positive but tends to zero with the particle diameter. The presence of particles produces a lag in the fluid velocity and the effect of such a drag can be interpreted as an effectively increased viscosity for the fluid-solid mixture.

8. DNS data can be sampled for average fluid and average solid velocities. The difference of these velocities is very small, but the difference between the composite velocity and the particle free Poiseuille flow is dramatic. We attempted to model the average flow of the slurry by a two-fluid model in which the particle laden region is treated as a fluid with an effective viscosity; for this calculation we used two different well regarded formulas for the effective viscosity with pure liquid above the mean height and effective liquid below. We would like to be able to predict the mean height from considerations involving an effective density.

Acknowledgement

This work was partially supported by the National Science Foundation KDI/New Computational Challenge grant (NSF/CTS-98-73236), by the US Army, Mathematics, the Engineering Research Program of the Office of Basic Energy Sciences at the DOE, by a grant from the Schlumberger foundation and from Stimlab Inc. and by the Minnesota Supercomputer Institute.

References

Choi, H.G. 2000 Splitting method for the combined formulation of fluid-particle problem. Accepted for Publication in *Comput. Meth Appl. Mech Engrg.*

Chorin A.J. 1968 Numerical solution of the Navier-Stokes equations. *Math. Comput*. **22**, 745-762.

Feng, J., Hu, H.H. & Joseph, D.D. 1994 Direct simulation of initial value problems for the motion of solid bodies in a Newtonian fluid. Part 1. Sedimentation. *J. Fluid Mech*. **261**, 95.

Iooss, G. & Joseph, D. D. 1990 *Elementary Stability and Bifurcation Theory*. Springer, Second Edition.

Joseph, D.D. 2000, Interrogations of direct numerical simulations of solid-liquid flow. *http://www.aem.umn.edu/Solid_Liquid-Flows/references.html.*

Kataoka, T., Kitano, T., Sasahara, M & Nishijima, K. 1978 Viscosity of particle filled polymer melts. *Rheol. Acta.* **17**, 149.

Kern, L.R., Perkins, T.K. & Wyant, R. E. 1959 The Mechanics of Sand Movement in Fracturing, *Petroleum Transactions*. AIME **216**, 403.

Patankar, N., Huang, Y., Ko, T & Joseph, D.D. 2000 Lift-off of a single particle in Newtonian and viscoelastic fluids by direct numerical simulation. Submitted to *J. Fluid Mech.*

Richardson, J.F. & Zaki, W. N. 1954 Sedimentation and Fluidization: Part I, *Trans. Instn. Chem. Engrs.* **32**, 35.

Thomas, D.G. 1965 Transport characteristics of suspension: VIII. A note on the viscosity of Newtonian suspension of uniform spherical particles. *J. Colloid Sci.* **20**, 267.

Wallis, G.B. 1969 *One-dimensional Two-phase Flow*. New York, McGraw-Hill.